

PHASE EQUILIBRIA OF Bi-Te-RE (Yb, Nd, Sm, Er, Tb) TERNARY SYSTEMS AT 673 K

L.-G. Zhang ^{a*}, Q. Song ^a, M.-Y. Tan ^a, Y. Jiang ^b, L.-B. Liu ^{a,c*}^a School of Material Science and Engineering, Central South University, Changsha, Hunan, China^b Hunan Institute for Drug Control, Changsha, Hunan, China^c Key Laboratory of Non-ferrous Metallic Materials Science and Engineering, Ministry of Education, Changsha, Hunan, China

(Received 18 November 2021; accepted 10 May 2022)

Abstract

The phase equilibria of Bi-Te-RE (Yb, Nd, Sm, Er, Tb) at 673 K were established through equilibrated alloys. The isothermal sections of Bi-Te-RE (Yb, Nd, Sm, Er, Tb) at 673 K were established according to the result of Scanning Electron Microscopy (SEM), Electron probe micro-analysis (EPMA), and Powder X-ray diffractometry (XRD). In the Bi-Te-Yb system at 673 K, the existence of 4 three-phase equilibria ($YbTe+Bi_2Te_3+Te$, $YbTe+Bi_2Te_3+\beta$, $YbTe+Bi+\beta$, $YbTe+Yb_3Bi_3+Yb_4Bi_3$) was established, while 3 three-phase regions ($NdTe_2+\beta+Bi_2Te_3$, $NdTe_2+\beta+Bi$, $Nd_2Te_3+Bi+BiTeNd$) in Bi-Te-Nd system, 3 three-phase regions ($SmTe_3+Te+Bi_2Te_3$, $SmTe_{1.8}+Bi_2Te_3+\beta$, $SmTe_{1.8}+\beta+Bi$) in Bi-Te-Nd system, 3 three-phase regions ($TbTe_3+Te+Bi_2Te_3$, $Tb_4Te_7+Bi_2Te_3+\beta$, $TbTe+Bi+\beta$) in Bi-Te-Nd system, and 4 three-phase regions ($ErTe_3+Te+Bi_2Te_3$, $ErTe_3+Bi_2Te_3+Er_2Te_3$, $Bi_2Te_3+Er_2Te_3+\beta$, $Er_2Te_3+\beta+ErTe$, $\beta+ErTe+Bi$) in Bi-Te-Nd system were also identified, respectively. Among the Bi-Te-RE (Nd, Sm, Er, Tb, Yb) systems, the solubilities of RE in Bi_2Te_3 were 0.19 at % Nd, 0.22 at % Sm, 0.28 at % Tb, 0.35 at % Er, and 0.37 at % Yb. In general, the maximum solubility of elements in Bi_2Te_3 phase alloy became larger with the increase in RE atomic number. A ternary compound $BiTeNd$ in the Bi-Te-Nd ternary system was confirmed in this work.

Keywords: Bi-Te alloy based alloys; Rare earth elements; EPMA; XRD; Isothermal section**1. Introduction**

Most commercial thermoelectric material near room temperature is Bi_2Te_3 -based thermoelectric material (TE) [1-2], which has been widely used in thermoelectric refrigeration, thermoelectric power generation, thermoelectric temperature control, thermoelectric sensors and other fields [3-4]. However, the application of Bi_2Te_3 -based thermoelectric material is limited at present due to its low thermoelectric figure of merit (ZT). Doping rare earth-metals (RE) is considered to be one of the most basic methods [5-6] to improve the ZT of Bi_2Te_3 based TE materials. The 1% addition of rare earth metals into the TE matrix can increase the ZT of thermoelectric material by 25% [7-8]. And it is also reported that rare earth elements (Yb, Ce, Sm and Er etc.) can improve the ZT of Bi_2Te_3 -based alloys [9-11]. The reason is that the rare earth atoms enter the materials lattice, and then produce a large local lattice distortion. Based on these, the solubility of doped rare earth atoms can largely affect the properties of TE

materials [12]. The information of solubility can always be clearly displayed in phase diagram [13-17]. Given all of that, to design Bi-Te based TE materials, it is imperative to study the phase diagrams of Bi-Te-RE systems [18-19]. In this work, the phase equilibria of Bi-Te-RE (Yb, Nd, Sm, Er, Tb) ternary systems at 673K were studied.

2. Literature review**2.1. Binary systems**

The experimental and thermodynamic studies on Bi-Te system have been conducted recently by our group [20]. In addition to Bi_2Te_3 , the existence of β phase with a large range of solid solubility at low temperatures was also confirmed. The crystal structure of Bi_2Te_3 is shown in Table 1.

Experimental and thermodynamic studies of Bi-RE (RE=Yb, Nd, Sm, Er, Tb) system have been carried out already [21-25]. The crystal structures of the intermetallic phases of these systems are listed in Table 1.

* Corresponding author: ligangzhang@csu.edu.cn; pdc@csu.edu.cn



Table 1. Intermetallic phases in the Bi-Te-RE (RE= Yb, Nd, Sm, Er, Tb) systems

System	Phase	Person symbol	Space group	Lattice parameters			Ref.
				a(nm)	b(nm)	c(nm)	
Bi-Te	Bi ₂ Te ₃	<i>hR15</i>	R-3m h	0.4395	0.4395	3.044	[20]
Bi-Yb	Yb ₅ Bi ₂	<i>oP*</i>	Pna21	1.236	0.828	0.966	[21]
	Yb ₄ Bi ₃	<i>cI28</i>	I-43d	0.9573	-	-	[21]
	YbBi ₂	<i>oS12</i>	Cmcm	0.456	1.668	0.428	[21]
	Yb ₅ Bi ₃	<i>oP32</i>	Pnma	12.638	0.9722	0.8407	[21]
Bi-Nd	NdBi ₂	<i>o*48</i>	*	0.647	11.864	12.982	[22]
	NdBi	<i>cF8</i>	Fm-3m	0.64222	-	-	[22]
	Nd ₄ Bi ₃	<i>cI28</i>	I-43d	0.95543	-	-	[22]
	Nd ₅ Bi ₃	<i>hP16</i>	P63/mcm	0.93696	-	-	[22]
	Nd ₂ Bi	<i>tI12</i>	I4/mmm	0.45603	-	17.865	[22]
	Bi-Sm	SmBi	<i>cF8</i>	Fm-3m	0.635	-	-
SmBi ₂		<i>o**</i>	*	0.642	1.164	1.28	[23]
Sm ₅ Bi ₃		<i>hP16</i>	P63/mcm	0.93	-	0.648	[23]
Sm ₂ Bi		<i>tI12</i>	I4/mmm	0.452	-	1.76	[23]
Sm ₄ Bi ₃		<i>cI28</i>	I-43d	0.94	-	-	[23]
Bi-Er	Er ₅ Bi ₃	<i>oP32</i>	Pnma	0.809	0.9349	11.806	[24]
	ErBi	<i>cF8</i>	Fm-3m	0.62023	-	-	[24]
Bi-Tb	Tb ₅ Bi ₃	<i>hP16</i>	P63/mcm	0.91006	-	0.63651	[25]
	Tb ₅ Bi ₃	<i>oP32</i>	Pnma	0.817	0.9487	11.968	[25]
	TbBi	<i>cF8</i>	Fm-3m	0.62759	-	-	[25]
	Tb ₄ Bi ₃	<i>cI28</i>	I-43d	0.93215	-	-	[25]
Te-Yb	YbTe	<i>cF8</i>	Fm-3m	0.6345	-	-	[21]
Te-Nd	NdTe	<i>Fm-3m</i>	Fm-3m	0.62839	0.62839	0.62839	[26]
	Nd ₂ Te ₃	<i>Pnma</i>	Pnma	121.856	0.43869	118.687	[27]
	NdTe ₂	<i>tP6</i>	P4/nmm O2	0.4377	0.4377	0.906	[27]
	Nd ₂ Te ₅	<i>oS28</i>	Cmcm	0.4409	4.41	0.4409	[27]
	NdTe ₃	<i>oS16</i>	Cmcm	0.43629	258.515	0.43469	[27]
Te-Sm	SmTe ₂	<i>tP6</i>	P4/nmm O2	0.437	0.437	0.9	[26]
	Sm ₂ Te ₃	<i>cI28</i>	I-43d	0.9506	-	-	[26]
	SmTe	<i>cF8</i>	Fm-3m	0.6595	-	-	[26]
Te-Er	ErTe ₃	<i>oS16</i>	Cmcm	0.431	2.545	0.431	[28]
	ErTe	<i>cF8</i>	Fm-3m	0.6063	-	-	[28]
Te-Tb	TbTe	<i>cF8</i>	Fm-3m	0.6101	-	-	[28]
	Tb ₂ Te ₃	<i>oF80</i>	Fddd O2	0.8679	12.276	26.037	[28]
	TbTe ₃	<i>oS16</i>	Cmcm	0.431	2.552	0.431	[29]

Compared with Bi-RE system, the phase diagram information of Te-RE (RE=Yb, Nd, Sm, Er, Tb) system is very limited. Although the thermodynamic

optimization of Te-Yb and Te-Sm binary systems was proposed [21, 26], only the rough phase diagrams of Te-Nd and Te-Er were obtained [27-28]. So far, there



was no phase diagram of Te-Tb system, only three intermetallic compounds were reported [29].

2.2. Ternary systems

Hulliger [30] reported $\text{Yb}_4\text{Bi}_2\text{Te}$ phase in his work. Later, Aliev et al. [31] reported two other ternary compounds: YbBi_4Te_7 and YbBi_2Te_4 . However, there is no experimental data or other evidence to prove the existence of these three compounds. The quasi-binary sections $\text{YbTe-Bi}_2\text{Te}_3$ were studied recently by Aliev et al. [32], in which YbBi_4Te_7 and YbBi_2Te_4 were still not confirmed. The group of researchers gathered for the study has recently studied the isothermal section of the Bi-Te-Yb system at 573K [33]. But at this temperature, no ternary compounds were found.

So far, there is no report on the relationship of Bi-Te-RE (RE= Nd, Sm, Er, Tb) ternary systems. Here in this work, the isothermal sections of Bi-Te-RE (RE= Nd, Sm, Er, Tb) systems at 673K were studied by means of SEM, EPMA, and XRD.

3. Experimental procedure

The isothermal sections of Bi-Te-RE (RE= Yb, Nd, Sm, Er, Tb) system were measured at 673K. Te has strong volatility, and there is a big gap between the melting points of RE-elements and the other two elements. Taking these into account, Bi_2Te_3 alloy was selected as the raw material to stabilize Te and reduce the melting point difference. The alloy samples of the three systems were prepared by Bi_2Te_3 rods (99.99%, Beijing Global Jinding Technology Co., Ltd.), Yb/Nd/Sm/Er/Tb blocks (99.9%, Hunan Rare Earth Metal Research Institute), and necessary Te blocks (99.99%, Beijing Global Jinding Technology Co., Ltd.) or Bi blocks (99.99%, Beijing Global Jinding Technology Co., Ltd.). The sample was sealed in a quartz tube filled with argon after vacuumizing. The Yb samples were melted in a box furnace at 950 °C for 5 hours, the Yb, Nd and Sm samples were melted at 1200 °C for 7 hours, the Er and Tb samples were melted at 1300 °C for 10 hours, and then cooled in the furnace. The uniform and pollution-free samples were sealed again in the vacuum quartz tubes for heat treatment. After annealing, the alloy was quenched in ice water. In order to avoid the loss of Te caused by long-term annealing, the actual composition of annealed samples was analyzed by chemical titration technique.

The microstructure and phase composition of the alloy were analyzed by scanning electron microscope (SEM, TESCAN MIRA3 LMH, 15 kV, working distance of 15 mm, Brno, The Czech Republic) and electron probe microanalysis (EPMA, JAXA-8800R, JEOL, 15 kV, 1×10^{-8} A, Tokyo, Japan). It should be noted that the rare earth mesophase is easy to oxidize,

so the polished samples needed to be characterized as soon as possible. The sample was analyzed by X-ray diffraction (XRD, Rigaku d-max/2550 VB, Cu K, 40 kV, 250 mA, Tokyo, Japan).

4. Results and discussion

4.1. The Bi-Te-Yb system

A series of samples were prepared to determine the phase relationships of the Bi-Te-Yb system in 673K isothermal sections. The chemical composition of the ternary alloy samples, as well as the composition of all phases and the forming phases in the sample, are included in Table 2.

Table 2. Phase composition and microanalysis of Bi-Te-Yb samples annealed at 673K

Alloy	Composition (at%)			Annealing	Phase composition (at%)			Phase
	Yb	Bi	Te		Yb	Bi	Te	
A1	10.0	21.2	68.8	673 K	0.04	1.10	98.86	(Te)
				40 days	50.57	0.37	49.06	YbTe
					0.36	38.61	61.03	Bi_2Te_3
A2	6.0	37.8	56.2	673 K	49.38	0.41	50.21	YbTe
				60 days	0.37	39.76	59.87	Bi_2Te_3
					0.39	46.97	52.64	β
A3	16.1	33.5	50.4	673 K	49.31	0.37	50.32	YbTe
				60days	0.41	50.47	49.12	β
A4	22.3	31.0	46.7	673 K	49.24	0.33	50.43	YbTe
				60 days	0.38	56.03	43.59	β
A5	31.7	27.5	40.8	673 K	49.54	0.35	50.11	YbTe
				60 days	0.39	59.09	40.52	β
					2.36	95.53	2.11	(Bi)
A6	56.8	28.9	14.3	673 K	50.43	0.37	49.20	YbTe
				40 days	62.58	34.26	3.16	Yb_3Bi_3
					57.20	39.96	2.84	Yb_4Bi_3
A7	8.4	33.3	58.3	673 K	49.60	0.23	50.17	YbTe
				40 days	0.37	38.69	60.94	Bi_2Te_3

Figure 1a shows the microstructure of alloy A1($\text{Yb}_{10}\text{Bi}_{21.2}\text{Te}_{68.8}$). BSE analysis showed that it contained a three-phase region, i.e. dark Te phase, white Bi_2Te_3 phase, and gray YbTe phase. According to EPMA analysis, the solubility of Yb in Bi_2Te_3 was 0.36 at %. The microstructure of A2 is shown in Figure 2a. BSE results showed that A2 alloy was composed of dark gray YbTe phase, gray Bi_2Te_3 phase, and white phase β . In Figure 2b, dark spots could be found in the dark gray YbTe phase, which was the oxidized YbTe phase.



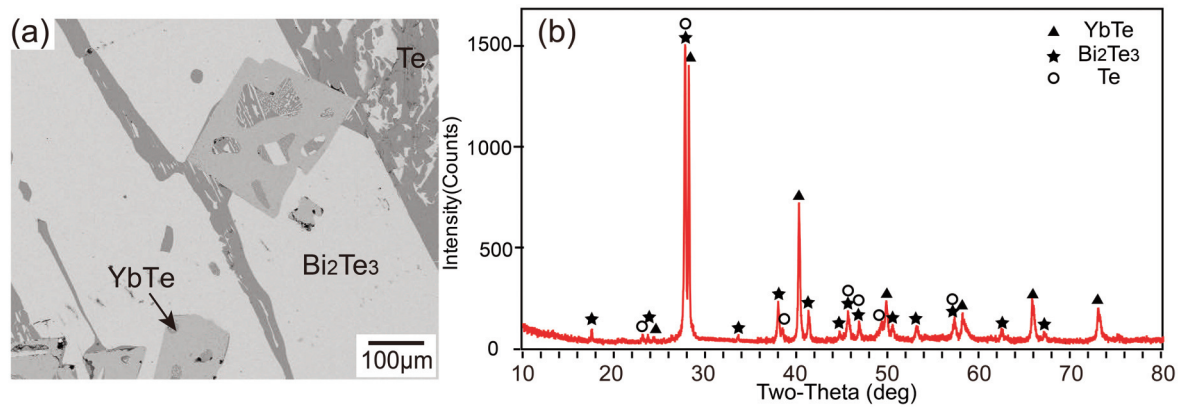


Figure 1. (a) BSE image and (b) XRD pattern of annealed alloy sample A1: $\text{Yb}_{10}\text{Bi}_{21.2}\text{Te}_{68.8}$

The XRD results of A1 and A2 alloys are shown in Figure 1b and Figure 2b, which further confirmed the two three-phase regions of $\text{YbTe}+\text{Bi}_2\text{Te}_3+\text{Te}$ and $\text{YbTe}+\text{Bi}_2\text{Te}_3+\beta$. The results of these two samples further confirmed that there existed no Te_2Yb and Te_3Yb_2 phases at 673K, which was consistent with the previous work at 573K [33].

Figure 3 shows the experimental results of A3 and A5 alloys. The microstructure of A3 sample showed the two-phase region of $\text{YbTe} + \beta$ (dark gray YbTe phase and white β phase). BSE analysis showed that A5 alloy was in the three-phase region ($\text{YbTe} + \text{Bi} + \beta$), as shown in Figure 3c. The results from XRD are shown in Figure 3b and Figure 3d. According to EPMA analysis, the solubility of Yb in β was about 0.4 at%.

This variation was in good agreement with the previous results of Bi-Te binary system [20] and Bi-Te-Yb isothermal section at 573K [33].

Alloy A6 ($\text{Yb}_{56.8}\text{Bi}_{28.9}\text{Te}_{14.3}$) was melted and annealed at 673K for 40 days. This alloy was prepared to confirm the existence of $\text{Yb}_4\text{Bi}_2\text{Te}$ phase reported by Hulliger [30]. According to the result of SEM, EPMA, and XRD, a three-phase region,

$\text{YbTe}+\text{Yb}_5\text{Bi}_3+\text{Yb}_4\text{Bi}_3$, existed as shown in Figure 5. According to these experimental information, $\text{Yb}_4\text{Bi}_2\text{Te}$ phase was found to be unstable at 673K.

At the same time, A7 alloy was prepared to confirm the existence of YbBi_2Te_4 . The microstructure and XRD results of the samples are shown in Figure 6. YbTe and Bi_2Te_3 coexisted in the sample. In this sample, the dark phase was YbTe and the gray phase was Bi_2Te_3 . According to the information in Figure 6, the YbBi_2Te_4 phase also could not be stabilized at 673K.

As shown in Figure 7, the 673K isothermal section of Bi-Te-Yb ternary system was constructed from the results of microstructure observation and phase analysis (including X-ray diffraction, SEM and EPMA analysis). It can be seen from Figure 7 that at 673K, four three-phase areas were identified in Bi-Te-Yb system, namely $\text{YbTe}+\text{Bi}_2\text{Te}_3+\text{Te}$, $\text{YbTe}+\text{Bi}_2\text{Te}_3+\beta$, $\text{YbTe}+\text{Bi}+\beta$, $\text{YbTe}+\text{Yb}_5\text{Bi}_3+\text{Yb}_4\text{Bi}_3$, and three three-phase areas could be inferred, namely $\text{YbTe}+\text{Bi}+\text{YbBi}_2$, $\text{YbTe}+\text{YbBi}_2+\text{Yb}_{11}\text{Bi}_{10}$ and $\text{YbTe}+\text{Yb}_4\text{Bi}_{23}+\text{Yb}_{11}\text{Bi}_{10}$. The maximum solid solubility of Yb in Bi_2Te_3 and β at 673 K was determined at about 0.4 at%. The Te_2Yb and Te_3Yb_2

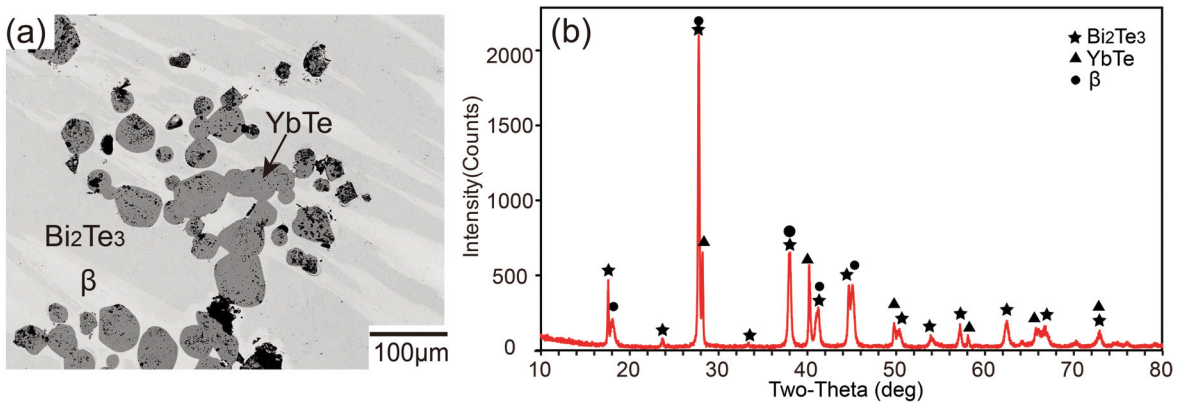


Figure 2. (a) BSE image and (b) X-ray powder diffraction pattern of annealed alloy sample A2: $\text{Yb}_6\text{Bi}_{37.8}\text{Te}_{56.2}$

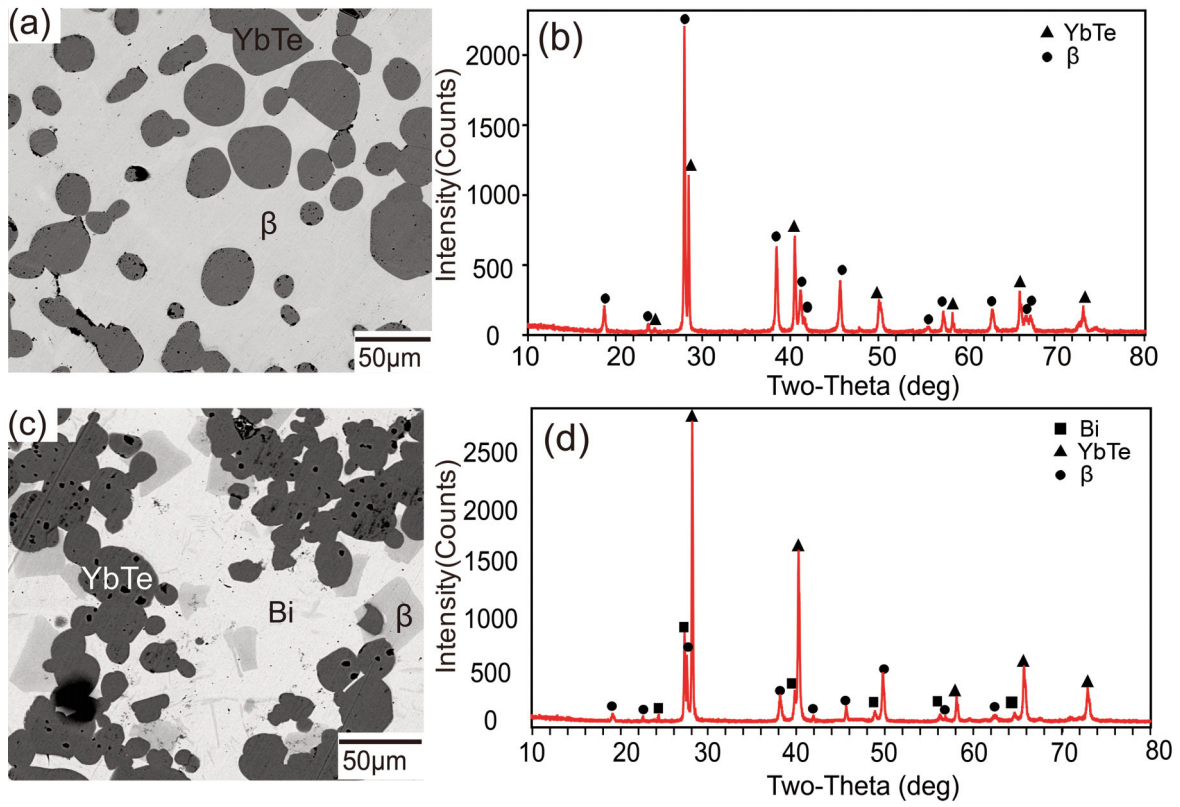


Figure 3. (a) BSE image and (b) XRD pattern of A3: $Yb_{16.1}Bi_{33.5}Te_{50.4}$ (c) BSE image and (d) XRD pattern of A5: $Yb_{31.7}Bi_{27.5}Te_{40.8}$

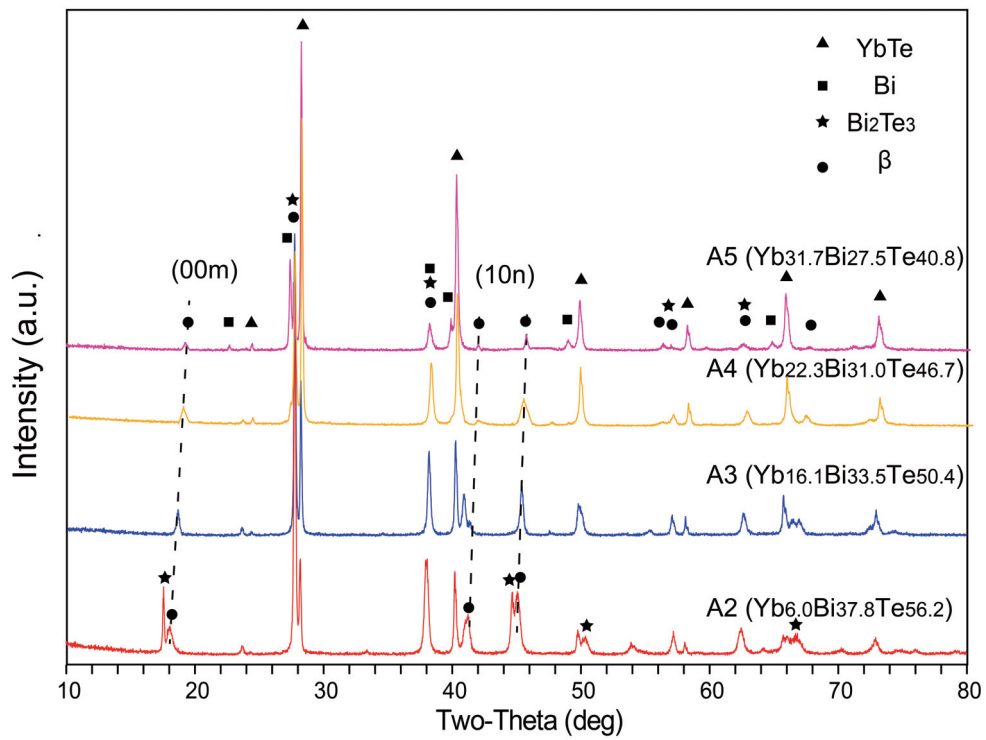


Figure 4. XRD patterns of equilibrated annealed samples A2-A5



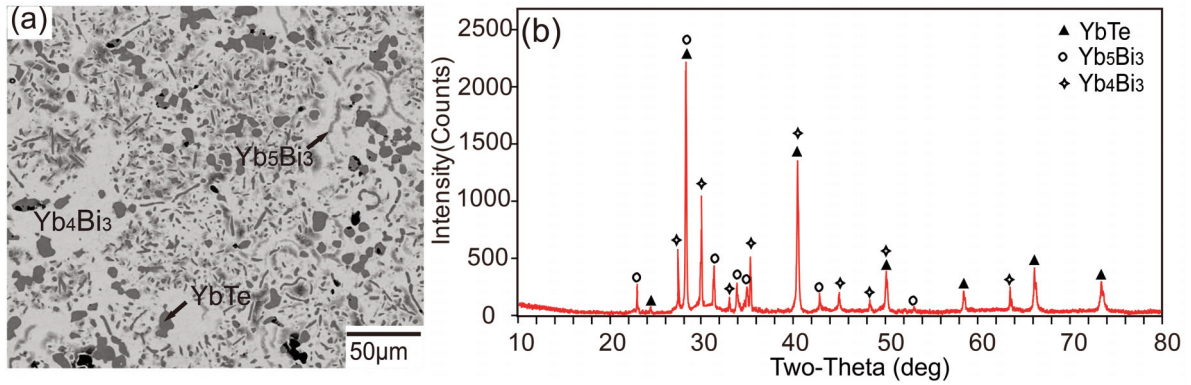


Figure 5. (a) BSE image and (b) XRD pattern of annealed alloy sample A6: $Yb_{56.8}Bi_{28.9}Te_{14.3}$

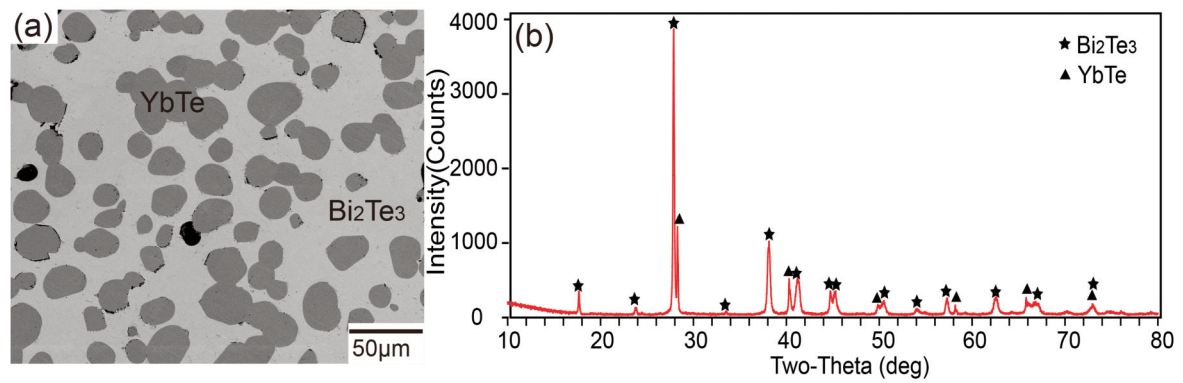


Figure 6. (a) BSE image and (b) XRD pattern of annealed alloy sample A7: $Yb_{8.4}Bi_{33.3}Te_{58.3}$

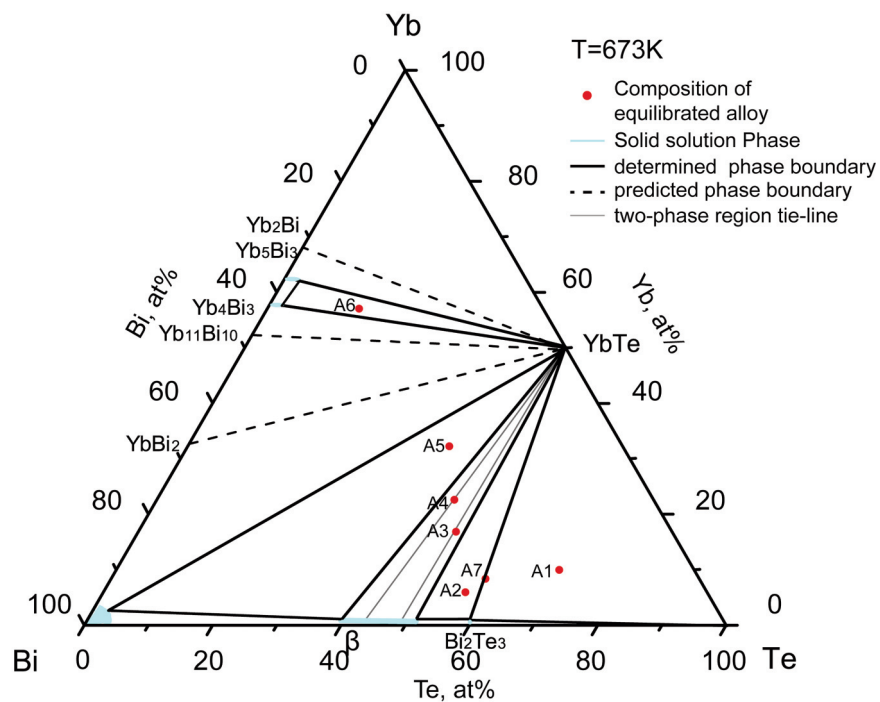


Figure 7. Experimentally determined 673K isothermal section of Bi-Te-Yb system

phases were not stable at this temperature. At 673K, there was no ternary compound in the Bi-Te-Yb ternary system.

4.2. The Bi-Te-Nd system

The 673K isothermal sections of Bi-Te-Nd system was determined by equilibrium alloy. Table 3 lists the chemical composition, all phases formed in the sample and their composition of Bi-Te-Nd ternary alloy sample.

Table 3. Phase composition and microanalysis of Bi-Te- Nd samples annealed at 673K

Alloy	Composition (at%)			Annealing	Phase composition (at%)			Phase
	Nd	Bi	Te		Nd	Bi	Te	
Nd								
N1	5.1	38.0	56.9	673 K	0.19	40.63	59.18	Bi ₂ Te ₃
				60 days	0.18	47.2	52.62	β
					35.49	0.19	64.32	NdTe ₂
N2	20.1	31.7	48.2	673 K	0.18	59.87	39.95	β
				60 days	35.29	0.26	64.45	NdTe ₂
					0.17	99.36	0.47	(Bi)
N3	31.2	27.5	41.3	673 K	41.36	0.01	58.63	Nd ₂ Te ₃
				60 days	35.99	33.69	30.32	BiTeNd
					0.09	99.44	0.47	(Bi)

The electron probe and X-ray diffraction results of two typical annealed samples (N2 and N3) of Bi-Te-Nd system are shown in Figure 8, including two three-phase regions, β+NdTe₂+Bi and Nd₂Te₃+BiTeNd+Bi. The structure and morphology of the alloy sample N2

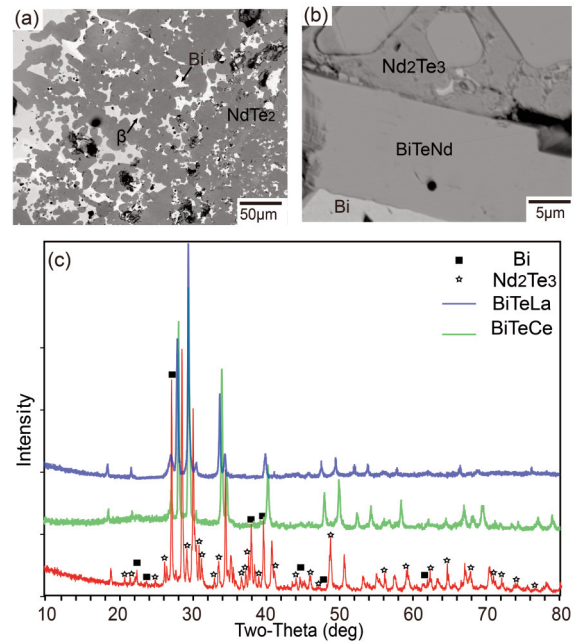


Figure 8. (a) BSE image of N2: Nd_{20.1}Bi_{31.7}Te_{48.2}, (b) BSE image and (c) XRD pattern of annealed alloy N3 : Nd_{31.2}Bi_{27.5}Te_{41.3}

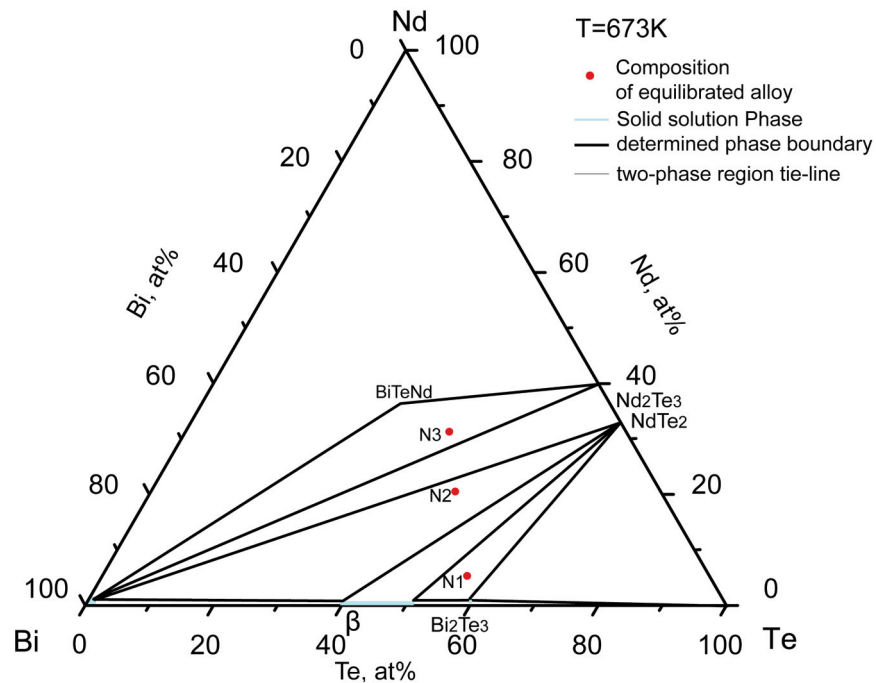


Figure 9. Experimentally determined 673K isothermal section of Bi-Te-Nd ternary system



(Fig. 8a) were similar to the corresponding La and Ce systems, but the NdTe_2 phase had no dark watermark [33]. The reason for this phenomenon was that these two elements could not be dissolved in the NdTe_2 phase. BiTeNd is a ternary compound, which was also found in the annealed samples of La and Ce systems (as the BiTeLa and BiTeCe compounds) [33]. The BSE image and XRD spectrum of the BiTeNd are shown in Figure 8a and 8b. As shown in Figure 8c, after matching the peaks corresponding to other two phases (Nd_2Te_3 and Bi) in the X-ray diffraction pattern of N3 alloy, the remaining peaks were matched with the X-ray diffraction peaks of BiTeLa and BiTeCe obtained in the previous work [33]. The results showed that the peaks of the corresponding peaks of BiTeLa were related to the peaks of the corresponding peaks of BiTeNd . The smaller the radius, the more it would drift to the right. For this reason, reference values for X-ray diffraction patterns were used to verify the reliability of the three atomic compounds, i.e. BiTeLa , BiTeCe , and BiTeNd . According to the results of microstructure observation and phase analysis, as shown in Figure 9, the 673K isothermal section of Bi-Te-Nd ternary system was illustrated.

4.3. The Bi-Te-Sm system

Table 4 list the EPMA results of three typical Bi-Te-Sm system annealed samples S1-S3.

Table 4. Phase composition and microanalysis of Bi-Te- Sm samples annealed at 673K

Alloy	Composition (at%)			Annealing	Phase composition (at%)			Phase
	Sm	Bi	Te		Sm	Bi	Te	
S1	5.1	38.0	56.9	673 K	0.22	41.19	58.59	Bi_2Te_3
				60 days	0.18	46.34	53.48	β
					35.40	0.20	64.40	SmTe_2
S2	11.8	35.3	52.9	673 K	35.75	0.55	63.70	SmTe_2
				60 days	0.15	58.73	41.12	β
S3	20.5	31.5	48.0	673 K	35.79	0.11	64.10	SmTe_2
				60 days	0.18	59.33	40.49	β
					1.32	1.01	97.67	(Bi)
S4	5.5	24.8	69.7	673 K	0.21	38.88	60.91	Bi_2Te_3
				60 days	24.80	0.13	75.07	SmTe_3
					0.22	0.17	99.61	(Te)

In all three samples, one phase had a chemical composition close to 36 at% Sm-64 at% Te (named as $\text{SmTe}_{1.8}$ or Sm_3Te_9 phase), which was designated as $\text{SmTe}_{1.8}$ phase at 673K according to the XRD spectrum of corresponding alloy samples. Back scattering (Figure 10a) and X-ray diffraction (Figure

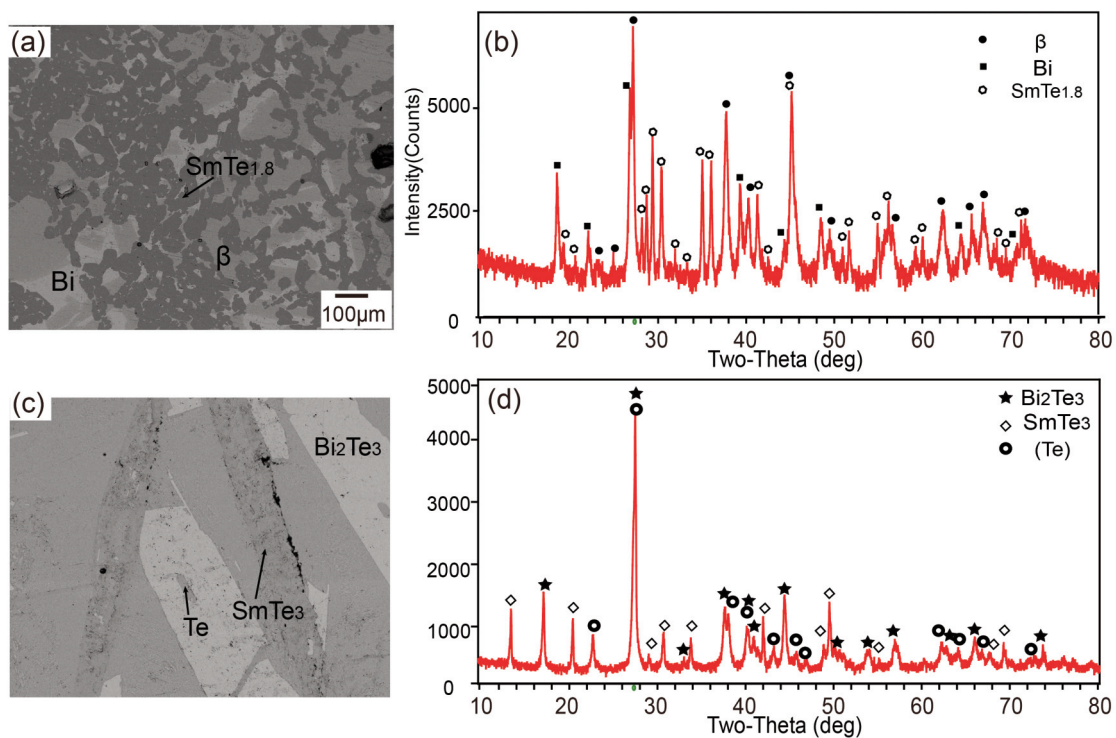


Figure 10. (a) BSE image and (b) XRD pattern of S3: $\text{Sm}_{20.5}\text{Bi}_{31.5}\text{Te}_{48}$, (c) BSE image and (d) XRD pattern of annealed alloy S4: $\text{Sm}_{5.5}\text{Bi}_{24.8}\text{Te}_{69.7}$

10b) showed the microstructure and X-ray diffraction peak of $\text{SmTe}_{1.8}$ phase of annealed sample S3, respectively. Although the reported phase diagram did not contain SmTe_3 phase [26], Figure 10c and 10d showed that SmTe_3 existed in SEM and EPMA results and XRD spectra of S4 alloy samples. According to the experimental results, the partial isothermal section of Bi-Te-Sm system is shown in Figure 11.

information of Te-Tb system, as shown in Table 5.

Figure 13a shows that the X-ray diffraction spectrum of the alloy sample T2 was in the three-phase region ($\text{Bi}+\beta+\text{TbTe}$). EPMA results of corresponding alloy samples confirmed this three-phase region (Table 3) as well. The results of XRD and BSE analysis showed that T3 alloy was located in the three-phase region of $\text{Bi}_2\text{Te}_3 + (\text{Te}) + \text{TbTe}_3$. Figure

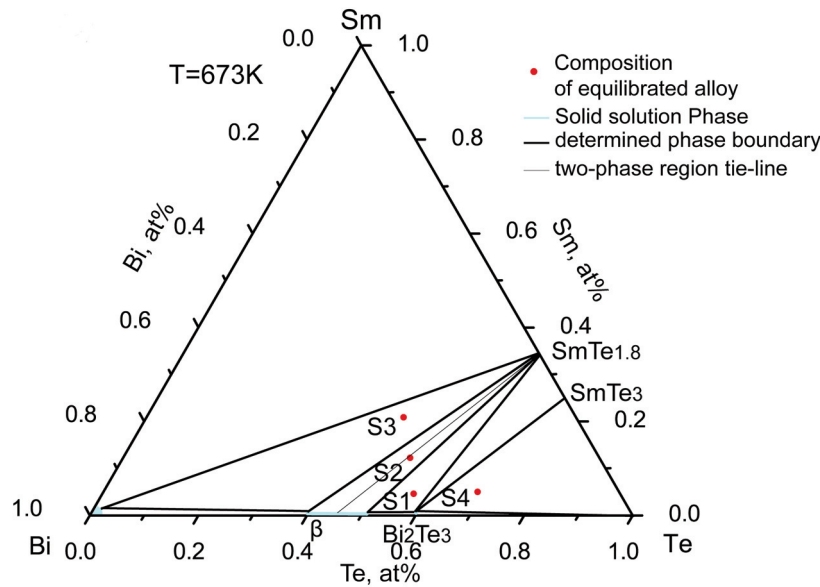


Figure 11. Experimentally determined 673K isothermal section of Bi-Te-Sm ternary system

4.4. The Bi-Te-Tb system

The experiment of Bi-Te-Tb system was mainly based on the phase structure information of Te-Tb system [29] due to the lack of phase diagram

Table 5. Phase composition and microanalysis of Bi-Te-Tb samples annealed at 673K

Alloy	Composition (at%)			Annealing	Phase composition (at%)			Phase
	Tb	Bi	Te		Tb	Bi	Te	
Nd								
T1	5.1	38.0	56.9	673 K	36.28	0.24	63.48	Tb_4Te_7
				60 days	0.24	48.55	51.21	β
					0.28	38.73	60.99	Bi_2Te_3
T2	29.2	28.1	42.7	673 K	49.12	0.11	50.77	TbTe
				60 days	0.24	58.96	40.80	β
					1.12	1.13	97.75	(Bi)
T3	5.5	24.8	69.7	673 K	0.27	38.72	61.01	Bi_2Te_3
				60 days	25.35	0.18	74.47	TbTe_3
					0.12	0.13	99.75	(Te)

13b is an XRD diagram of T3 alloy. The microstructure of T3 alloy was similar to that of other Te-rich samples (see Figure 1a). For annealed sample T1, the BSE results of Figure 13c indicated that there was a phase whose chemical composition was close to Tb_4Te_7 . But its crystal structure had not been reported. Figure 13d shows the XRD peak of the phase, which was related to the diffraction peak of RETe_2 . In addition, Ramsey [34] also pointed out that La_4Te_7 was very similar to LaTe_2 in structure in La-Te system. According to the chemical composition analysis, this phase had the same structure as LaTe_2 , which may be Tb_4Te_7 phase. The XRD evidence did not fully illustrate this result, so the Tb_4Te_7 legend in Figure 13d was gray (indicating uncertainty), which ment future research was needed. The three-phase regions of $\text{Bi}_2\text{Te}_3 + (\text{Te}) + \text{TbTe}_3$, $\text{Bi}_2\text{Te}_3 + \beta + \text{Tb}_4\text{Te}_7$, and $\beta + \text{Bi} + \text{Tb}_2\text{Te}_3$ were established according to three typical annealing samples of Bi-Te-Tb system. Figure 12 shows the isothermal section of Bi-Te-Tb the ternary system at 673K in the low rare earth region.

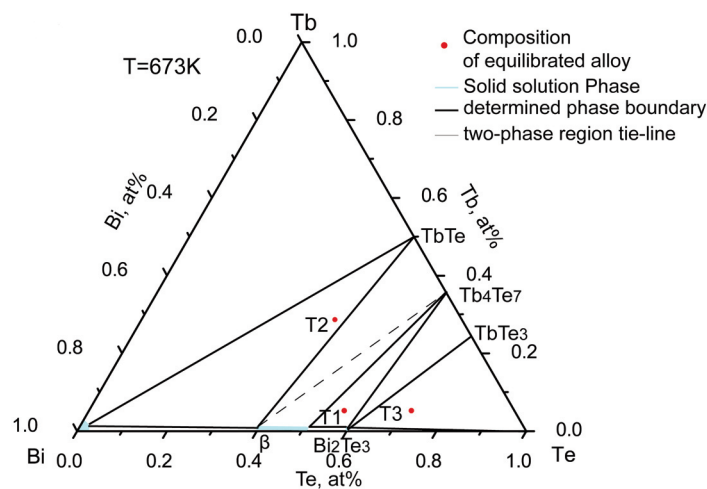
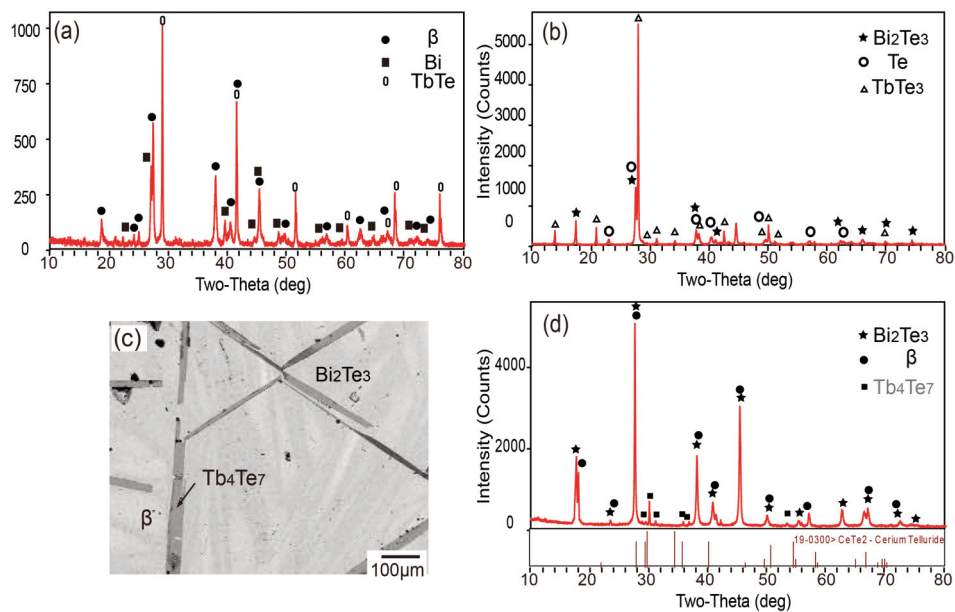
4.5. The Bi-Te-Er system

Table 6 lists the EPMA results of three typical Bi-



Table 6. Phase composition and microanalysis of Bi-Te-Er samples annealed at 673K

Alloy	Composition (at%)			Annealing	Phase composition (at%)			Phase
	Er	Bi	Te		Er	Bi	Te	
E1	5.1	38.0	56.9	673 K	0.35	40.04	59.61	Bi_2Te_3
				60 days	0.24	46.74	53.02	β
					39.82	0.71	59.47	Er_2Te_3
E2	21.5	31.1	47.4	673 K	0.26	59.40	40.34	β
				60 days	39.50	0.12	60.38	Er_2Te_3
E3	31.6	27.3	41.1	673 K	49.92	0.97	49.11	ErTe
				60 days	0.26	60.33	39.41	β
					49.74	2.30	47.96	ErTe
E4	5.5	24.8	69.7	673 K	1.32	1.21	97.47	(Bi)
				60 days	0.32	38.77	60.91	Bi_2Te_3
					25.55	0.38	74.07	ErTe_3

**Figure 12.** Experimentally determined 673K isothermal section of Bi-Te-Tb ternary system**Figure 13.** XRD pattern of (a) T2: $\text{Tb}_{29.2}\text{Bi}_{28.1}\text{Te}_{42.7}$ (b) T3: $\text{Tb}_{5.5}\text{Bi}_{24.8}\text{Te}_{69.7}$ (c) BSE image and (d) XRD pattern of annealed alloy T1: $\text{Tb}_{5.1}\text{Bi}_{38.0}\text{Te}_{56.9}$

Te-Er system annealed samples E1-E4.

Four three-phase regions were established based on SEM, EPMA, and XRD results of four Bi-Te-Er annealed samples, which were $\text{Bi}_2\text{Te}_3+\text{Te}+\text{ErTe}_3$, $\text{Bi}_2\text{Te}_3+\beta+\text{Er}_2\text{Te}_3$, $\text{Er}_2\text{Te}_3+\beta+\text{ErTe}$, and $\text{Bi}+\beta+\text{ErTe}$, and they contained all the compounds reported in Er-Te binary system [28]. The microstructure and XRD of typical sample E2 are shown in Figure 14a and 14b,

including dark gray Er_2Te_3 , gray ErTe , and white β . In addition, Er element was easier to oxidize than other rare earth metals, and the oxidation type was inter crystalline oxidation (Figure 14c). Therefore, sample detection should be fast and timely, and try to shorten the residence time in the air. The 673K isothermal section of Bi-Te-Er system is shown in Figure 15.

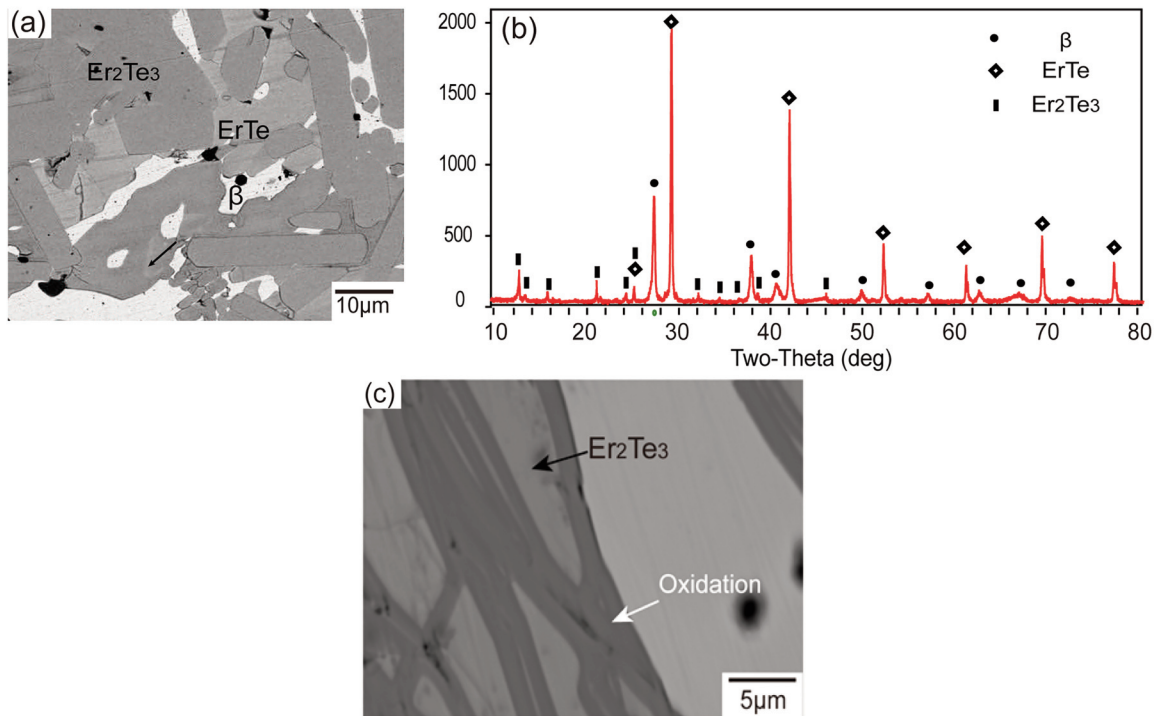


Figure 14. (a) BSE image and (b) XRD pattern of E2: $\text{Er}_{21.3}\text{Bi}_{31.1}\text{Te}_{47.4}$; (c) Oxidation morphology of Er_2Te_3 phase

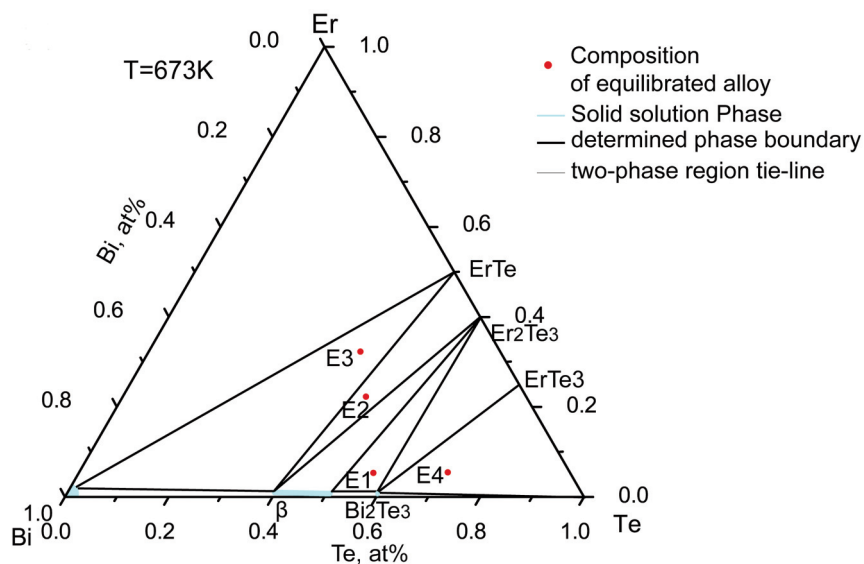


Figure 15. Experimentally determined 673K isothermal section of Bi-Te-Er ternary system

5. Conclusions

The 673K isothermal section of Bi-Te-RE (Yb, Nd, Sm, Er, and Tb) ternary system was determined by equilibrium alloy method, scanning Electron Microscopy, electron probe microanalysis, and X-ray powder diffraction. Through the comprehensive analysis of these five systems, it was found that with the decrease of the atomic radius of rare earth elements at 673K, the solid solubility of rare earth elements in Bi-Te matrix increased. The solubility of rare earth elements in Bi-Te alloy was very small, and the maximum solubility of Yb was 0.37 at.% at 673K. A ternary compound NdBiTe in the Bi-Te-Nd ternary system was confirmed.

Acknowledgements

This work is financially supported by National Natural Science Foundation of China (Grant No. 51871248, 51501229), Natural Science Foundation of Hunan Province, China (Grant No. 2020JJ4739) and the Guangxi Key Laboratory of Information Materials (Guilin University of Electronic Technology), China (Grant No. 201009-K).

Author contributions

Ligang Zhang: Investigation, Writing-original draft, Writing-review & editing. Qian Song: Methodology, Investigation, Writing-review & editing. Mingyue Tan: Methodology, Investigation. Yun Jiang: Methodology, Investigation. Libin Liu: Methodology, Investigation.

Data Availability

The data used to support the findings of this study are available from the corresponding author upon request.

Conflict of interest

The authors declare that they have no known conflict financial interests or personal relationships that could have appeared to influence the work reported in this paper.

References

- [1] F. J. DiSalvo, Thermoelectric Cooling and Power Generation, *Science*, 285 (5428) (1999) 703-706. <http://dx.doi.org/10.1126/science.285.5428.703>
- [2] V. L. Kuznetsov, L. A. Kuznetsova, A. E. Kaliazin & D. M. Rowe, High performance functionally graded and segmented Bi₂Te₃-based materials for thermoelectric power generation, *Science*, 37(2002) 2893-2897. <https://doi.org/10.1023/A:1016092224833>
- [3] H.P. Hu, K.Y. Xia, T.J. Zhu, X.B. Zhao, Recent Advances in Ag-Based Superionic Thermoelectric Materials, *Chinese Journal of Rare Metals*, 45(2021) 513-529. <https://doi.org/10.13373/j.cnki.cjrm.XY20070024>
- [4] Q.F. Chen, X.X. Wang, Z.S. Wu, C.Y. Liu, L. Miao, Recent Advances in SnSe-Based Thermoelectric Materials, *Chinese Journal of Rare Metals*. 44(2020) 1316-1324. <https://doi.org/10.13373/j.cnki.cjrm.XY19050002>
- [5] P. Liu, L.C. Liu, H.R. Gong, Stacking fault energy and electronic structure of molybdenum under solid solution softening/hardening, *Journal of Central South University*, 28(2021) 39-41. <https://doi.org/10.1007/s11771-021-4584-2>
- [6] K.F. Chen, P. Cai, H.L. Peng, X.G. Xue, Z.M. Wang, L.X. Sun, Ti₃C₂T_x MXene for organic/perovskite optoelectronic devices, *Journal of Central South University*, 28(2021) 3935-3958. <https://doi.org/10.1007/s11771-021-4846-z>
- [7] E.M. Levin, S.L. Bud'ko, K. Schmidt-Rohr, Enhancement of Thermopower of TAGS-85 High-Performance Thermoelectric Material by Doping with the Rare Earth Dy, *Advanced Functional Materials*, 22(2012) 2766-2774. <https://doi.org/10.1002/adfm.201103049>
- [8] E.M. Levin, R. Hanus, M. Hanson, W.E. Straszheim, K. Schmidt-Rohr, Thermoelectric properties of Ag₂Sb₂Ge_{46-x}Dy_xTe₅₀ alloys with high power factor, *Physica Status Solidi*, 210(2013) 2628-2637. <https://doi.org/10.1002/pssa.201330217>
- [9] H.J.V. Daal, P.B.V. Aken, K.H.J. Buschow, The seebeck coefficient of YbAl₂ and YbAl₃, *Physics Letters A*, 49(1974) 246-248. [https://doi.org/10.1016/0375-9601\(74\)90870-6](https://doi.org/10.1016/0375-9601(74)90870-6)
- [10] E.M. Levin, B.S. Kuzhel, O.I. Bodak, B.D. Belan, I.N. Stets, Concentrated Kondo Systems in Solid Solutions on the Base of Europium Ternary Compounds, *Physica Status Solidi*, 161(2010) 783-795. <https://doi.org/10.1002/pssb.2221610233>
- [11] L.M. Goncalves, C. Couto, P. Alpuim, J.H. Correia, Optimization of thermoelectric properties on Bi₂Te₃ thin films deposited by thermal co-evaporation, *Thin Solid Films*, 518(2010) 2816-2821. <https://doi.org/10.1016/j.tsf.2009.08.038>
- [12] E.M. Levin, B.A. Cook, J.L. Harringa, S.L. Bud'ko, R. Venkatasubramanian, K. Schmidt-Rohr, Analysis of Ce- and Yb-Doped TAGS-85 Materials with Enhanced Thermoelectric Figure of Merit, *Advanced Functional Materials*, 21(2011) 441-447. <https://doi.org/10.1002/adfm.201001307>
- [13] L.H. Zheng, L.G. Zhang, F.Y. Zhao, L.B. Liu, D. Wang, C.J. Wu, Phase Equilibria of the Al-Co-Er System at 400°C and 600°C, *Journal of Mining and Metallurgy Section B-Metallurgy*, 57(2021) 359-370. <https://doi.org/10.2298/JMMB210317032Z>
- [14] Y. Jiang, F. Li, S.R. Li, K. Xu, L.L. Chen, X.Z. Deng, Y.Y. Huang, K. Chang, Thermodynamic Assessment of the Fe-Nb-Si System, *Journal of Mining and Metallurgy Section B-Metallurgy*, 57(2021) 331-340. <https://doi.org/10.2298/JMMB210220029J>
- [15] F.Y. Zhao, L.G. Zhang, H. Wang, L.B. Liu, Phase equilibria investigation of the Al-Ni-Er ternary system at 600 °C and 700 °C, *CALPHAD*, 75(2021) 102353. <https://doi.org/10.1016/j.calphad.2021.102353>
- [16] Z.T. Du, L. Zhou, C.P. Guo, X.P. Ren, C.R. Li,



- Experimental investigation and thermodynamic description of the Fe–Mo–Zr system, CALPHAD, 74(2021) 102314. <https://doi.org/10.1016/j.calphad.2021.102314>
- [17] C.B. Li, Q. Song, X.W. Yang, Y.D. Wei, Q. Hu, L.B. Liu, L.G. Zhang, Experimental Investigation of the Phase Relations in the Fe-Zr-Y Ternary System, Materials, 15(2022) 593. <https://doi.org/10.3390/ma15020593>
- [18] B. Kumar, C.S. Tiwary, M.K. Paek, M. Paliwal, Thermodynamic modelling of the ternary Bi-Ga-Te system for potential application in thermoelectric materials, CALPHAD, 74(2021) 102326. <https://doi.org/10.1016/j.calphad.2021.102326>
- [19] E.T. Dong, S.H. Tan, J. Wang, W.S. Liu, W.Q. Zhang, Thermodynamic activity of solute in multicomponent alloy from first-principles: Excess Mg in Mg-3(Sb1-xBix)(2) as an example, CALPHAD, 74(2021) 102318. <https://doi.org/10.1016/j.calphad.2021.102318>
- [20] C.Mao, M. Tan, L. Zhang, D. Wu, W. Bai, L. Liu, Experimental reinvestigation and thermodynamic description of Bi-Te binary system, CALPHAD, 60(2018) 81-89. <https://doi.org/10.1016/j.calphad.2017.11.007>
- [21] J.S.Wang, Y.N. Yue, C.R. Li, C.P. Guo, Z.M. Du, B. Wu, Thermodynamic assessments of the Yb–Bi and the Yb–Te systems, CALPHAD, 51(2015) 306-313. <https://doi.org/10.1016/j.calphad.2015.10.007>
- [22] C.P.Wang, H.L. Zhang, A.T. Tang, F.S. Pan, X.J. Liu, Thermodynamic assessments of the Bi–Nd and Bi–Tm systems, Journal of Alloys and Compounds, 502(2010) 43-48. <https://doi.org/10.1016/j.jallcom.2010.03.042>
- [23] H. Okamoto, Bi-Sm (Bismuth-Samarium), Binary Alloy Phase Diagrams, 2nd ed., Ohio: ASM International, USA, 1990, p. 794-795. <https://doi.org/10.31399/asm.hb.v03.a0006247>
- [24] J.S.Wang, C.R. Li, C.P. Guo, Z.M. Du, B. Wu, Thermodynamic assessment of the Bi–Er and the Bi–Dy systems, Thermochemica Acta, 566(2016) 44-49. <https://doi.org/10.1016/j.tca.2013.05.024>
- [25] S.L.Wang, Z.B. Hu, F. Gao, C.P. Wang, X.J. Liu, Thermodynamic Assessments of the Bi-Tb and Bi-Y Systems, Journal of phase equilibria and diffusion, 32(2011) 441-446. <https://doi.org/10.1007/s11669-011-9939-1>
- [26] G.Chattopadhyay, J.M. Juneja, A thermodynamic database for tellurium-bearing systems relevant to nuclear technology, Journal of Nuclear Materials, 202(1993) 10-28. [https://doi.org/10.1016/0022-3115\(93\)90024-S](https://doi.org/10.1016/0022-3115(93)90024-S)
- [27] H.Okamoto, Nd-Te (Neodymium-Tellurium), Binary Alloy Phase Diagrams, 2nd ed., Ohio: ASM International, USA, 1990; p. 2814-2817. <https://doi.org/10.31399/asm.hb.v03.a0006247>
- [28] D.J.Haase; H. Steinfink; E.J. Weiss, The Phase Equilibria and Crystal Chemistry of the Rare Earth Group VI Systems. II. Erbium-Tellurium, Inorganic Chemistry, 4(4)(1965) 4541-4543. <https://doi.org/10.1021/ic50026a021>
- [29] B. Predel. Tb-Te, Landolt-Börnstein - Group IV Physical Chemistry 5J (Pu-Re – Zn-Zr), 1st ed., Heidelberg: Springer-Verlag Berlin, Germany, 1998, pp. 1.
- [30] F.Hulliger, F. Levy, Layered Structures. (Book Reviews: Structural Chemistry of Layer-Type Phases), Science, 35(1979) 793. <https://www.science.org/doi/10.1126/science.198.4321.1030.a>
- [31] O.M. Aliev, T.F. Maksudova, N.D. Samsonova, L.D. Finkel'shtein, P.G. Rustamov, Synthesis and Properties of Compounds of the Type A(Iii)B(Vi)2x(Vi)4, A(Iii)B(V)4x(Vi)7 And A(Iii)3b(V)4x(Vi)9, Inorg. Mater. (translated from Neorg. Mater.), 22 (1986) 23-27.
- [32] Z.S.Aliev, K.D. Rasulova, I.R. Amiraslanov, J.C. Tedenac, M.B. Babanly, Phase diagram of the YbTe–SbTe–BiTe quasi-ternary system 2323, Journal of Alloys & Compounds, 589(2014) 399-404. <https://doi.org/10.1016/j.jallcom.2013.11.225>
- [33] M.Y. Tan, C. Mao, L.G. Zhang, W.M. Bai, L.B.Liu, Experimental investigation of phase relations in Bi-Te-RE (Yb, La, Ce) ternary systems, CALPHAD, 61(2018) 62-71. <https://doi.org/10.1016/j.calphad.2018.02.007>
- [34] T.H. Ramsey, H. Steinfink, E.J. Weiss, The Phase Equilibria and Crystal Chemistry of the Rare Earth-Group VI Systems. IV. Lanthanum-Tellurium, The Phase Equilibria and Crystal Chemistry of the Rare Earth-Group VI Systems. IV. Lanthanum-Tellurium, Inorganic Chemistry, 4(1965) 1154-1157. <https://doi.org/10.1021/ic50030a014>



FAZNE RAVNOTEŽE U Bi-Te-RE (Yb, Nd, Sm, Er, Tb) TROJNIM SISTEMIMA NA 637 K

L.-G. Zhang ^{a*}, Q. Song ^a, M.-Y. Tan ^a, Y. Jiang ^b, L.-B. Liu ^{a,c*}

^a Fakultet za nauku o materijalima, Centralno-južni univerzitet, Čangša, Hunan, Kina

^b Institut za kontrolu lekova u provinciji Hunan, Čangša, Kina

^c Glavna laboratorija za nauku i inženjerstvo materijala od obojenih metala. Ministarstvo prosvete, Čanša, Hunan, Kina

Apstrakt

Fazna ravnoteža Bi-Te-RE (Yb, Nd, Sm, Er, Tb) na 637 K je uspostavljena pomoću ravnotežnih legura. Izotermni preseki Bi-Te-RE (Yb, Nd, Sm, Er, Tb) su utvrđeni na osnovu rezultata SEM, EPMA i XRD analize. U sistemu Bi-Te-Yb na 637 K je ustanovljeno postojanje 4 trofaznih ravnoteža ($YbTe+Bi_2Te_3+Te$, $YbTe+Bi_2Te_3+\beta$, $YbTe+Bi+\beta$, $YbTe+Yb_3Bi_3+Yb_4Bi_3$), 3 trofazna regiona ($NdTe_2+\beta+Bi_2Te_3$, $NdTe_2+\beta+Bi$, $Nd_2Te_3+Bi+BiTeNd$) u Bi-Te-Nd sistemu, 3 trofazna regiona ($SmTe_3+Te+Bi_2Te_3$, $SmTe_{1,8}+Bi_2Te_3+\beta$, $SmTe_{1,8}+\beta+Bi$) u Bi-Te-Sm sistemu, 3 trofazna regiona ($TbTe_3+Te+Bi_2Te_3$, $Tb_4Te_7+Bi_2Te_3+\beta$, $TbTe+Bi+\beta$) u Bi-Te-Tb sistemu i 4 trofazna regiona ($ErTe_3+Te+Bi_2Te_3$, $ErTe_3+Bi_2Te_3+Er_2Te_3$, $Bi_2Te_3+Er_2Te_3+\beta$, $Er_2Te_3+\beta+ErTe$, $\beta+ErTe+Bi$) u Bi-Te-Er sistemu. Među Bi-Te-RE (Nd, Sm, Er, Tb, Yb) sistemima, rastvorljivost RE u Bi_2Te_3 iznosila je 0,19 za % Nd, 0,22 za % Sm, 0,28 za % Tb, 0,35 za % Er, i 0,37 za % Yb. Rezultati su pokazali da je maksimalna rastvorljivost elemenata u Bi_2Te_3 fazi legure postignuta sa povećanjem atomskog broja RE. Potvrđeno je postojanje trojnog jedinjenja $BiTeNd$ u Bi-Te-Nd trojnom sistemu.

Ključne reči: Legure na bazi Bi-Te; Retki elementi; EPMA; XRD; Izotermni presek

